## ARTICLE

Check for updates

# Non-linear coherent perfect absorption in the proximity of exceptional points

Suwun Suwunnarat[1], Yaqian Tang[1], Mattis Reisner[2], Fabrice Mortessagne[2], Ulrich Kuhl [2✉] &
Tsampikos Kottos [1✉]

Coherent perfect absorption is one of the possibilities to get high absorption but typically suffers from being a resonant phenomena, i.e., efficient absorption only in a local frequency range. Additionally, if applied in high power applications, the understanding of the interplay of non-linearities and coherent perfect absorption is crucial. Here we show experimentally and theoretically the formation of non-linear coherent perfect absorption in the proximity of exceptional point degeneracies of the zeros of the scattering function. Using a microwave platform, consisting of a lossy nonlinear resonator coupled to two interrogating antennas, we show that a coherent incident excitation can trigger a self-induced perfect absorption once its intensity exceeds a critical value. Note, that a (near) perfect absorption persists for a broadband frequency range around the nonlinear coherent perfect absorption condition. Its origin is traced to a quartic behavior that the absorbance spectrum acquires in the proximity of the exceptional points of the nonlinear scattering operator.

[1] Wave Transport in Complex Systems Lab, Physics Department, Wesleyan University, 06459 Middletown, CT, USA. [2] Université Côte d'Azur, CNRS, Institut de Physique de Nice (INPHYNI), 06108 Nice, France. ✉email: ulrich.kuhl@univ-cotedazur.fr; tkottos@wesleyan.edu

Perfect absorption of the energy carried by a classical wave is an interdisciplinary research theme spanning areas as diverse as acoustics and mechanical waves[1,2], to radio-frequency[3], microwaves[4,5] and optical wave settings[6–10]. At the core of this activity is the promise that perfect absorption can be beneficial to a variety of applications ranging from stealth technologies[3,11,12], energy harvesting and photovoltaics[13], sensing[14,15], and photodetection[16,17]. Along these lines, the quest for low-cost/power all-optical switching and modulation schemes that simultaneously utilize coherent interaction of light beams and absorbing matter for extreme absorption is recently gaining a lot of attention[18–20]. One such protocol is the so-called coherent perfect absorption (CPA).

Coherent perfect absorption (CPA) is a multichannel wave-form shaping protocol that leads to the complete extinction of a monochromatic radiation when it enters a weakly lossy cavity[10,21,22]. Although the scheme has been initially proposed in the framework of classical optics[21,22], as the time-reversed process of a laser, it turns out that its implementation does not require time-reversal symmetry[23–25]. It rather solely relies on wave interference effects that entrap the incident radiation inside the lossy cavity, leading to its complete absorption. Such mechanism allows us to control light with light in a linear fashion, through just the relative phases and amplitudes of the multiple inputs. Subsequent studies nicely demonstrated the CPA implementation, beyond the original platform of optics[8,18,20,22,26–30], spanning all areas of classical wave physics ranging from microwave[25,31,32] and RF[33], to acoustics[34,35]. In all the above-mentioned cases, the CPA protocol demonstrated a narrow, resonant-based, (perfect) absorption with very sharp characteristics around the frequency of perfect absorbance. Obviously, addressing this "deficiency" will open up a whole range of possibilities for the CPA scheme including solar pho-tovoltaic or stealth applications.

At the same time, most of the CPA studies and their imple-mentations have been performed that underlying wave systems were linear, i.e., under the assumption of scale invariance. The absence of implementation of CPA protocols in wave systems that lack scale invariance comes as a surprise, specifically since non-linear mechanisms are abundant in nature and they offer additional degrees of freedom for light manipulation. Only recently, some researchers[36–38] have put forward the question of the applicability of a CPA scheme in cases where scale invariance is violated. The reasons for this lack of effort to identify non-linear CPA (NLCPA) protocols are two-fold: From the theoretical side, one needs to develop computational schemes since the well-established (linear) scattering formalism is not anymore applic-able. Moreover, in the presence of non-linear interactions one needs to control, not only the relative phases and amplitudes of the incident waves but also their absolute magnitude. From the experimental side, one might question the viability of such pro-tocols due to bi-stabilities and other non-linearity-driven phe-nomena which might destroy the delicate interferences between various propagating waves, or result in modulation instabilities making the NLCPA concept unrealistic. It is therefore imperative to test the implementation of a non-linear CPA protocol (if at all realizable) under experimental conditions.

In this paper, we introduce an electromagnetic platform, con-sisting of microwave resonators, where an NLCPA with broad-band characteristics can be investigated theoretically and imple-mented experimentally. The absence of scale invariance and the dependence of the scattering process from the absolute magni-tude of the incident wave amplitudes result in a self-induced CPA with a variety of photonic applications in areas like signal pro-cessing, non-linear interferometry, and sensing. In the case of perfect coupling of the resonators with the interrogating

antennas, the system supports a different type of NLCPA modes which demonstrate a square-root frequency degeneracy in the neighborhood of a critical magnitude of the incident wave amplitudes– remnant of an exceptional point (EP) degeneracy occurring in linear non-hermitian systems. EP degeneracies have been documented in the non-Hermitian literature as a main source of wave phenomena ranging from loss-induced transpar-ency and unidirectional invisibility, to parity-time-symmetric lasers, and hypersensitive sensors (for some recent reviews see[39–42]). Here, we provide a paradigm of EP degeneracies associated with steady-state non-linear solutions of the wave operator, with incoming boundary conditions, that are respon-sible for a broad-band (near-) perfect absorption.

## Results and discussion

**Experimental setup**. The experimental setup (Fig. 1a) consists of a dielectric resonator coupled to a short-circuited diode (Fig. 1b) sandwiched between two aluminum plates. This hybrid system demonstrates a non-linear response[43,44]. The resonator is excited via two kink antennas curved around it. The antennas excite the first TE-resonance mode of the resonator (around 6.7 GHz), where the magnetic field $\vec{B}$ has only a z-component and the electric field lies parallel to the aluminum plates. The magnetic field couples to the short-circuited diode thus inducing a non-linear behavior of the system. The incident and reflected waves of the system are separated by circulators connected to the source cable, the antenna, and the measuring port of the vector network analyzer (VNA). The excitation, with power $P_{VNA}$, is injected from port 1 of the VNA and it is splitted equally by a T-junction going through the In-phase and Quadrature (IQ) vector mod-ulators into the circulators. The IQ-modulators allow to vary the power and phase difference between the excitation lines. Thus the measured complex transmission amplitudes from port 1 to port 2 $S_{21}$ and to port 3 $S_{31}$ of the VNA give access to the reflected power of the system $R = |S_{21}|^2 + |S_{31}|^2$. The total absorbance is then given by $A = 1 - R = 1 - |S_{21}|^2 - |S_{31}|^2$ where the scattering matrix elements $|S_{21}|^2$ and $|S_{31}|^2$ have been normalized taking into account the absorbance due to the IQ-modulator, the cables, and the circulators (see "Methods" section).

The power of the incident signals $P_{IQ1}$ and $P_{IQ2}$, injected from each of the two antennas are controlled by the power injected from the VNA $P_{VNA}$ (maximal accessible $P_{VNA} = 10$ dBm), and by a differential absorption $\mathcal{P}_{IQ1}$ and $\mathcal{P}_{IQ2}$ associated to each of the two IQ-modulators adjoint to the two antennas. The same IQ-modulators can also tune the relative phases $\phi_{IQ1}$ and $\phi_{IQ2}$ of each of the two incident waves. Finally, the couplings between the resonator and the two antennas have been treated as free parameters and they have been adjusted by curving the horizontal part of the kink antennas (Fig. 1) and/or by appropriately positioning the dielectric resonator in their proximity (see supplementary note 1 and supplementary fig. 1).

**Theoretical model**. The transport characteristics of a system of coupled resonators are modeled using a time-independent cou-pled mode theory (CMT)

$$\omega \psi_n = H_{n,n-1} \psi_{n-1} + H_{n,n+1} \psi_{n+1} + H_{n,n} \psi_n, \qquad (1)$$

where $\omega$ is the frequency of the incident monochromatic wave, $\psi_n$ is the scattering magnetic field amplitude represented in the TE-modes of the individual resonator (Wannier basis) localized at the n-th resonator[45], $H_{n,n+1} = H_{n+1,n}^*$ describes the coupling between the n-th and n + 1-th resonators and $H_{n,n} = \epsilon_n$ is the resonant frequency of the n − th resonator. For the specific case of Fig. 1a the scattering system consists of only one resonator at n = 0. The two semi-infinite chains of coupled resonators with n ≠ 0 have the
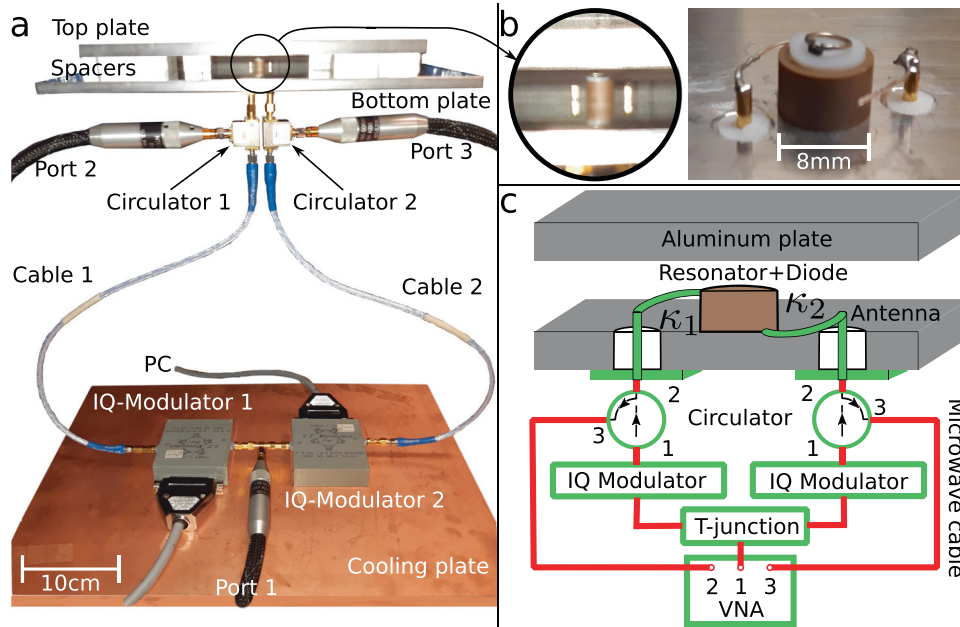
**Fig. 1 The experimental setup. a** Photograph of the experimental system including the connections. The scale is given on the lower left. **b** Zoom showing the experimental non-linear system consisting of a cylindrical dielectric resonator (permittivity $\epsilon_r \approx 36$, radius = 4 mm, height = 5 mm) where a short-circuited diode is situated above separated by a 1 mm high Teflon spacer (permittivity $\epsilon_r = 2.1$ with the two transmitting/receiving antennas, where the distance between the central parts of the antennas is 15 mm. The resonator is sandwiched between two aluminum plates with a distance 16 mm. The scale given corresponds to the diameter of 8 mm of the resonator. **c** Sketch detailing the setup. IQ-modulator stands for In-phase and Quadrature vector modulators, VNA for Vector Network Analyzer, PC for Personal Computer, and $\kappa_1$ and $\kappa_2$ for the coupling strengths of the antennas. The coaxial cables have a length of 50 cm.

same resonant frequency $\epsilon_n = \epsilon \approx 6.7$ GHz and model the left and right antennas (leads). They are coupled with one another via a (real) coupling constant $H_{n,n+1} = \nu$ giving rise to a dispersion relation $\omega = \epsilon + 2\nu \cos(k)$ ($k \in [0, 2\pi]$ is the wave-vector of a propagating wave). The coupling strength between the non-linear resonator ($n = 0$) with the left ($n < 0$) and to the right ($n > 0$) leads are $H_{-1,0} = \kappa_1 = |\kappa_1| e^{-i\phi_1}$ and $H_{0,1} = \kappa_2 = |\kappa_2| e^{-i\phi_2}$, respectively. The non-linear resonator at site $n = 0$, has a resonant frequency $\epsilon_0 = \epsilon + \Omega(|\psi_0|^2)$. The complex function $\Omega(|\psi_0|^2) = \Omega_r(|\psi_0|^2) + i\Omega_i(|\psi_0|^2)$ depends on the local field intensity $|\psi_0|^2$. Measurements of one-sided transmission measurements indicated that the best fit with the predictions of the model of equation (1) are achieved when

$$\Omega(|\psi_0|^2) \approx \beta_0 + \beta_1 |\psi_0|^2, \quad (2)$$

where $\beta_0 = (67.74 + 3i)$ MHz, $\beta_1 = (-0.141 + 0.41i)$ MHz mW$^{-1}$ while $\nu = 0.1$ GHz.

The most general solution of equation (1) in the left and right leads, can be written as

$$\psi_n = \begin{cases} I_1 e^{ikn} + R_1 e^{-ikn} & n < 0 \\ I_2 e^{-ikn} + R_2 e^{ikn} & n > 0 \end{cases}, \quad (3)$$

where $I_{1,2}$ are given by the scattering boundary conditions and represent the amplitudes of a left/right incident waves. Substituting the above expressions in equation (1) for $n = 0$, we get:

$$\left[\omega - \Omega\left(|\psi_0|^2\right)\right]\psi_0 = \kappa_1^*\left(I_1 e^{-ik} + R_1 e^{ik}\right) + \kappa_2\left(I_2 e^{-ik} + R_2 e^{ik}\right). \quad (4)$$

An additional relation between $R_{1,2}$ and $I_{1,2}$ is derived by substituting equation (3) back in equation (1) for $n = \pm 1$. We have that

$$\psi_0 = \frac{\nu}{\kappa_1}\left(I_1 + R_1\right) = \frac{\nu}{\kappa_2^*}\left(I_2 + R_2\right), \quad (5)$$

which allows us to express equation (4) in terms of the monochromatic frequency $\omega$ and the amplitudes $I_{1,2}$ and $R_{1,2}$ of the counter-propagating waves in each of the two leads.

A CPA protocol inhibits all outgoing waves, i.e., $R_1 = 0 = R_2$. Imposing these constrains in equation (5) allows us to express $\psi_0$ as $\psi_0 = \frac{\nu}{\kappa_1}I_1 = \frac{\nu}{\kappa_2^*}I_2$. This relation indicates that the field $\psi_0$ (and therefore the non-linear losses $\Omega(|\psi_0|^2)$) is controlled by the couplings and the incident amplitudes $I_{1,2}$ of the incoming waves while it remains unaffected by $\omega$. A re-arrangement of the above relation into an expression for the relative amplitudes leads us to the conclusion that a potential CPA occurs only if the condition $I_2 = \frac{\kappa_2^*}{\kappa_1}I_1$ is satisfied.

For symmetric couplings with $|\kappa_1| = |\kappa_2| = \kappa_0$ we have $I_2 = I_1 e^{i\phi}$ where the relative phase is $\phi = (\phi_1 + \phi_2)$. When we substitute these expressions in equation (4), together with the CPA constraint $R_1 = R_2 = 0$, we arrive at a transcendental equation with respect to $\omega$, whose (complex) roots are functions of the incident field intensity $|I_1|^2$ and can be associated with an NLCPA. In fact, only their real value subset (if any!) of these $\omega$-roots are physically admissible CPA solutions as they are the only ones that satisfy the incoming boundary conditions (i.e., propagating waves). We point out that as opposed to the linear CPA, here the $I_1$ (or $I_2$) is treated as a free parameter that can enforce an NLCPA.

**Absorbance**. To confirm the efficiency of the NLCPA protocol, we first analyze the total absorbance $A(\omega; I_1, I_2)$:

$$A(\omega; I_1, I_2) \equiv 1 - \Theta(\omega; I_1, I_2); \ \Theta(\omega; I_1, I_2) = \frac{|R_1|^2 + |R_2|^2}{|I_1|^2 + |I_2|^2}, \quad (6)$$

where $\omega \in \mathcal{R}$ are the real frequencies of an incident monochromatic wave with left/right amplitudes $I_1$ and $I_2$, respectively. For one-side incident waveforms (e.g. $I_2 = 0$) the absorbance gets the
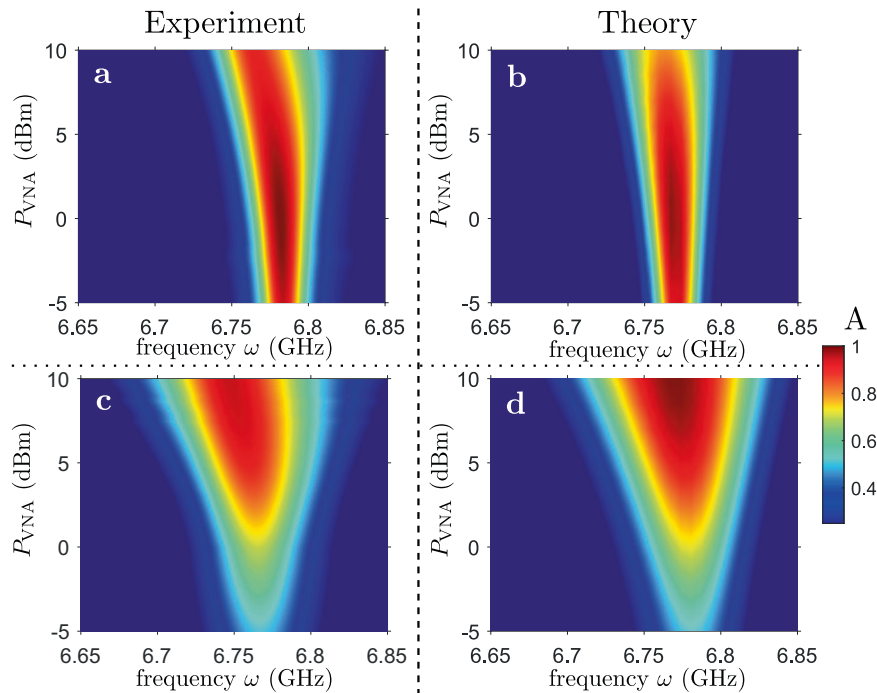
**Fig. 2 Absorbance $A$ as a function of frequency $\omega$ and the injected power $P_{VNA}$.** In **a** the experimentally measured absorption for two weakly coupled antennas with coupling strength, $\kappa_0 = 0.23$ GHz is shown. **b** shows the corresponding result of our modeling equation (1) with non-linear complex frequency shift $\Omega$ given by equation (2). The experimental maximal absorbance is $A = 99.99\%$ occuring at $P_{NLCPA} = 0$ dBm, $\omega_{NLCPA} \approx 6.782$ GHz. The theoretical NLPCA's gives $A = 1$, at $P_{NLCPA} = -0.486$ dBm, $\omega_{NLCPA} = 6.769$ GHz. The results for two moderately coupled antennas ($\kappa_0 = 0.4$ GHz) for the experiment (**c**) and the model (**d**) are shown. The experimental maximum absorbance is $A \approx 95\%$ occurring at $P_{NLCPA} = 9.8$ dBm, $\omega_{NLCPA} = 6.747$ GHz. The theoretical non-linear perfect coherent absorber (NLPCA) with $A = 1$, occurs at $P_{NLCPA} = 10.23$ dBm, $\omega_{NLCPA} = 6.77$ GHz.

expected form $A = 1 - |r|^2 - |t|^2$ where $|r|^2$, $|t|^2$ are the reflectance and transmittance respectively. In the multichannel case, the evaluation of $A(\omega; I_1, I_2)$ requires the knowledge of $R_1, R_2$ which, for a given set $\omega; I_1, I_2$, can be calculated via equations (4, 5). Note that the absorbance $A$ in equation (6) acquires the maximum value $A = 1$ whenever $R_1 = R_2 = 0$, i.e., when we have an NLCPA condition.

In order to minimize the available parameter space, we strived to achieve symmetric coupling amplitude configurations, i.e., $|\kappa_1| = |\kappa_2| = \kappa_0$. The latter has been guaranteed via weak power measurements (linear scattering regime), when the reflected signals at each antenna individually was measured to be the same. We have further simplified our interrogation scheme by setting $\mathcal{P}_{IQ1} = 1$ dB and $\phi_{IQ1} = 0$ while varying the amplitude and phase $\mathcal{P}_{IQ2}, \phi_{IQ2}$ (via the second IQ-modulator) of the injected signal through the second antenna together with the total absolute power $P_{VNA}$ controlled by the VNA. Finally, we have scanned the residual parameter space and measured for each of the varying parameters the transmissions $S_{21}$ and $S_{31}$ from which we extracted the total reflected power and absorbance $A$.

From the previous discussion, we expect that when $\sqrt{\mathcal{P}_{IQ1}/\mathcal{P}_{IQ2}} = |\kappa_1/\kappa_2| = 1$ the system might support an NLCPA at some critical incident power $P_{VNA}$. Of course, a necessary condition is that the extracted NLCPA frequency $\omega_{NLCPA}$ is real. To this end, we proceed with the analysis of the absorbance measurements for two settings associated with a weak and moderate coupling constants $\kappa_0$. In the former case, we find a set of parameters $P_{VNA} = 0$ dBm, $\mathcal{P}_{IQ1} = 5.0$ dB, $\mathcal{P}_{IQ2} = 5.7$ dB, and $\phi_{IQ2} = 92°$ for which $A \geq 99.99\%$ at $\omega_{NC} = 6.782$ GHz. The slight difference between left and right incident wave powers is attributed to the fact that $|\kappa_1/\kappa_2| \approx 1$. The same extreme absorption is found for moderate coupling constants, for which

$A \approx 95\%$. The corresponding NLCPA parameters are $\omega_{NC} = 6.747$ GHz, $P_{VNA} = 9.8$ dBm, $\mathcal{P}_{IQ1} = 5.0$ dB, $\phi_{IQ1} = 0°$, $\mathcal{P}_{IQ2} = 5.0$ dB, $\phi_{IQ2} = 83.5°$. In both cases, a shift of the maximal absorbance as a function of the incident power is observed showing that the non-linearity induces also a slight frequency shift. In Fig. 2a, c we report the measured absorbance as a function of frequency $\omega$ and incident power $P_{VNA}$. In these measurements, the relative phases of the incident waves were kept fixed, given by $\phi_{IQ2} = 92°$ and $\phi_{IQ2} = 83.5°$ for weak and moderate couplings respectively. The supplementary note 2 provides additional experimental evidence that variations of the relative phase (supplementary Figs. 2d and 3d) and amplitudes (supplementary Figs. 2c and 3c) of the incident waves result in an abrupt deterioration of the absorbance—thus underlying the delicate interferometric process between the two left and right monochromatic waves, also typical for linear CPAs. We, however, underline an additional feature of our non-linear CPA which is its dependence on the total incident power, (Fig. 2, supplementary Figs. 2b and 3b).

Next, we turn to the theoretical analysis of $A(\omega; I_1, I_2)$. In our modeling, $\kappa_1 = \kappa_0$ and $\kappa_2 = -i\kappa_0$ with $\kappa_0 = 0.23$ GHz for the weak and $\kappa_0 = 0.4$ GHz for the moderate couplings (Fig. 2b, d). We considered that $I_1 = I$ and $I_2 = e^{i\phi}I_1$ with relative phase $\phi = \pi/2$. Using equations (4, 5) we extracted numerically the corresponding $R_1, R_2$ and evaluated the absorption $A(\omega; I)$ using equation (6). We have achieved perfect absorption $A = 1$ at ($I_{NLCPA}$, $\omega_{NLCPA}$) corresponding to $(-0.48$ dBm, $6.769$ GHz) and $(10.23$ dBm, $6.770$ GHz) for weak and moderate coupling values $\kappa_0$ respectively. These results are in quantitative agreement with the experiment. A surprising feature of our calculations, which reproduces the behavior of the measured absorbance $A(\omega)$, is the broadening of the frequency range over which large absorption values are achieved as $\kappa_0$ approaches perfect coupling $\kappa_0 = v$. This
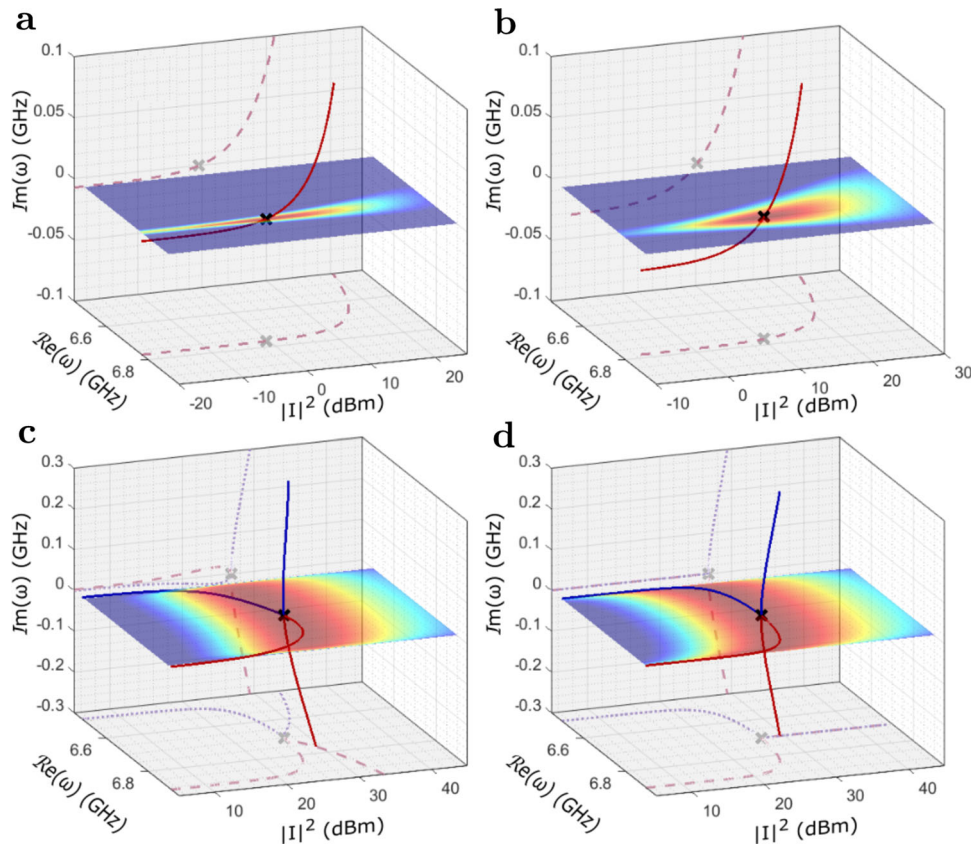
**Fig. 3 Complex zeros dependence on the input power for different coupling strength.** Trajectories (red and blue solid lines) of the complex zeros $\omega$ of the scattering matrix as a function of input power. The dashed and dotted lines are projections of these trajectories on the corresponding plane. The non-linearity $\Omega = \beta_0 + \beta_1 |\psi_0|^2$ with $\beta_0 = (67.74 + 3.00i) \times 10^{-3}$ GHz $\beta_1 = (-0.141 + 0.410i) \times 10^{-3}$ GHz mW$^{-1}$. **a** For two weakly coupled antennas of relative coupling strength $\kappa/\nu = 0.23$, where $\nu$ is the coupling strength inside the semi-infinite leads and $\kappa$ the coupling strength to the non-linear resonator. **b** For two intermediately coupled antennas of $\kappa/\nu = 0.40$. **c** For two perfectly coupled antennas $\kappa/\nu = 1$. **d** As bottom left but the real part of the non-linearity is set zero, i.e., no real frequency shift. The absorbance $A$ is reported as a density plot versus the frequency $\omega$ and the power $P_{\text{VNA}}$ injected by the vector network analyzer (VNA) using the same color scale is in Fig. 2.

domain appears to be in the vicinity of the NLCPA and tends to occur for larger $I_{\text{NLCPA}}$ values as $\kappa_0$ increase. For example, for $\kappa_0 = 0.4\,GHz$, one has that $A(\omega \in [\omega_{\text{NLCPA}} \pm 21\,\text{MHz}] > 80\%$ occurring at incident powers around $P_{\text{VNA}} \approx 10\,\text{dBm}$ which is the maximum power of our VNA.

**Absorption broadening due to EP degeneracies of NLCPAs.** To understand the origin of the broad-band high absorptivity we analyze the parametric evolution of the NLCPA frequencies versus the incident power $I$. By imposing the CPA conditions $R_1 = R_2 = 0$ and combining equations (4, 5) we arrive to the transcendental equation for $\omega_{\text{NLCPA}}$

$$f(\omega) = \Omega\left(\left|\frac{\nu}{\kappa_1} I_1\right|^2\right) + \frac{\kappa^2}{\nu} e^{-ik} - \omega = 0;\ \kappa^2 \equiv |\kappa_1|^2 + |\kappa_2|^2, \quad (7)$$

where $\omega(k) = 2\nu \cos(k)$. We re-iterate that physically acceptable NLCPA's correspond to the case where the $\omega_{\text{NLCPA}}$ roots of equation (7) are real, corresponding to propagating waves (supplementary note 3).

We consider the specific example of our system where the non-linear resonator takes the form of equation (2). The parametric evolution of the (complex) roots $\omega_{\text{NLCPA}}$ of equations (7) vs. the intensity of the incident wave $I = I_1 = I_2$ are shown in Fig. 3 (top) for a weak ($\kappa_0/\nu = 0.23$) and moderate ($\kappa_0/\nu = 0.4$) coupling constants. In the frequency range $\omega \in [6.5, 6.9]$ GHz (passband of

the leads), the equation (7) has only one complex root $\omega$ which crosses the real plane at the incident intensity $I_{\text{NLCPA}}$ resulting to maximum absorbance $A = 1$ (see density plots). This is a direct confirmation that the perfect absorption that we have found in our experiment is indeed associated with an NLCPA condition. From Fig. 3 (top) we see that higher (experimentally inaccessible) intensities of the incident waves suppress the absorbance as they lead to an enhanced impedance mismatch of the resonator. The redshift of the maximum absorbance is associated with the real part of the non-linear component of $\Omega(|\psi_0|^2)$. Another important conclusion of our analysis is that the critical coupling regime ($\kappa_0 = \nu$), enforces an $\omega - I$ parameter domain with high-absorbances. This result has been already demonstrated in Fig. 2 but now it is more prominent since we are able to analyze incident powers above 10 dBm (power limit of our VNA).

The situation is more challenging when we consider perfect coupling, i.e., $\kappa_0/\nu = 1$. In this case, equation (7) has two complex roots within the propagating band, (Fig. 3c). One of them (red trajectory) approaches the real plane from above, while the other one (blue trajectory) crosses the real plane from below as the intensity of the incident wave increases. At the crossing point (marked with a black cross) the two roots degenerate forming a self-induced EP degeneracy of CPAs. Its formation demonstrates all the characteristics of an EP singularity, known from the physics of linear non-Hermitian operators with the most prominent being a square-root singularity. Since the EP occurs
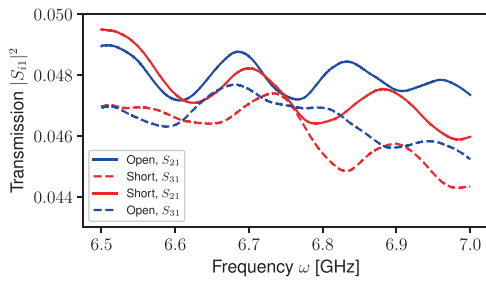
**Fig. 4 Transmission calibration.** Transmission intensities $|S_{21}^{(cal)}|^2$ and $|S_{31}^{(cal)}|^2$ where the non-linear system has been replaced by open and short terminations at the two antennas, respectively.

at the real $\omega$ − plane it constitutes a physically allowable CPA with absorbance $A = 1$. The latter, together with the fact that the two coalescing complex $\omega_{NLCPA}$ "trajectories" have small imaginary part (see dashed lines projected in the imaginary $\omega$ − plane), results to the appearance of a (near-)perfect (i.e. $A \geq 95\%$) absorption for a broad frequency range covering approximately 90% of the allowed propagation band of the leads. We stress that the broad-band absorption is counter-intuitive and challenges the understanding of CPA as a resonant phenomenon. It turns out that the broadband high-absorptivity is quite robust, forgiving small variations of the intensity $|I|^2$ with respect to the critical value.

To understand better the appearance of a broad-band high absorbance, we simplify further our critical coupling set-up by designing the non-linear diode characteristics in order to enforce the two complex-zero trajectories to fall onto the real plane. This is shown in Fig. 3 (lower right) where the non-linear parameters in equation (2) are taken to be $\beta_0 = 3.00i \times 10^{-3}$ GHz and $\beta_1 = 0.410i \times 10^{-3}$ GHz mW$^{-1}$. In this case, the square-root degeneracy of the NLCPAs $\omega_{NLCPA} - \omega_{EP} \sim \sqrt{|I_{EP}|^2 - |I|^2}$ occurs on the real-$\omega$ plane with $\omega_{EP} \approx 6.7$ GHz while $|I_{EP}|^2 \approx 27$ dBm as in lower left of Fig. 3. Such behavior leads to abrupt frequency variations in the vicinity of the $I_{EP}$, which span a frequency range as large as 90% of the available spectrum. Of course, once we move away from the critical $I_{EP}$-value (say at $|I|^2 = 15$ dBm), we recover the typical sharp CPA features with respect to detuning $\omega$ which are reflected in an abrupt drop in absorption for frequency detuning $\omega \neq \omega_{NLCPA}$.

We can quantify the broad-band absorption, by analyzing an effective "linear" model which describes the steady-state transport characteristics of our non-linear setting Fig. 1 in the proximity of the EP. Specifically, the EP scattering field $\psi_0$, determines the local losses $\Omega_0(|\psi_0|^2)$. The corresponding scattering matrix is

$$S(\omega) = -\hat{1} + \frac{2i \sin(k)}{\nu} W^\dagger \frac{1}{H_{eff} - \omega} W = -\hat{1} + \alpha W^\dagger W, \quad (8)$$

where $H_{eff} = \Omega_0 + \frac{e^{ik}}{\nu} W W^\dagger$, $W = (\kappa_1, \kappa_2)$ and $\alpha = \frac{1}{\nu^2} \frac{\sqrt{1-\delta\omega^2}}{1+\sqrt{1-\delta\omega^2}}$ (where $\delta\omega = \omega - \omega_{EP}$). In the last equality we assumed EP conditions, i.e., $\kappa_1 = \kappa_2 = \nu$. Note, that the condition equation (7) for the existence of CPA's is equivalent to the eigensolutions of the wave operator (described by $H_{eff}$) with incoming boundary conditions $(k \rightarrow -k)$, i.e., $\det[H_{eff}(-k) - \omega(k)] = 0$[23,25]. Therefore, we associate the EP-CPAs with the formation of EPs in the spectrum of $H_{eff}(-k)$. From equation (8) we have calculated the absorption matrix

$$A = 1 - S^\dagger S = \frac{2\alpha}{1 + \sqrt{1 - \delta\omega^2}} W^\dagger W$$

$$\approx \frac{1}{2\nu^2} \left(1 - \frac{1}{16}\delta\omega^4 + \mathcal{O}(\delta\omega^6)\right) W^\dagger W. \quad (9)$$

indicating a quartic broadening of the absorption spectrum in the neighborhood of $\omega_{EP}$[46] ($\frac{1}{2\nu^2} W^\dagger W$ has eigenvalues 1 and zero). The latter prediction is nicely reproduced by the results shown in Fig. 3.

## Conclusions

We demonstrated the viability of a self-induced coherent perfect absorber by utilizing a simple microwave setup consisting of a dielectric resonator inductively coupled to a non-linear diode. In the weak coupling regime, we have observed sharp (resonant-like) absorption up to 99.99% at the frequency of the NLCPA. As the coupling with the interrogating antennas is approaching the critical coupling regime, the frequency range where extreme absorption (>95%) occurred, increases dramatically leading to a broad-band (near-)perfect absorption in the neighborhood of the NLCPA. A CMT model describes the experimental findings nicely and shows that this broadening is attributed to the formation of self-induced exceptional point degeneracies associated with the NLCPA frequencies. It will be interesting to investigate more complex scenarios where the EP of the NLCPA frequencies is of higher order resulting (probably) in an even broader (near-) perfect absorption. Our results pave the way to applications of CPA in microwave/RF and optical regimes.

## Methods

The details of the experimental setup are given in the corresponding subsection. The experimental data have been acquired using a standard vector network analyzer using a full 12 term calibration. We additionally calibrated the measured transmission by measuring the scattering matrix elements $S_{21}^{(cal)}$ and $S_{31}^{(cal)}$ for the system shown in Fig. 1, where we attached either an open or a short terminator to port 2 of each circulator, thus replacing the connection to the non-linear system. In Fig. 4 the transmission intensities $|S_{i1}^{(cal)}|^2$ are shown for both open and short termination circuits. The incident power $P_{VNA}$ has been set to 10 dBm while all IQ-Modulators are arranged to provide power reduction which is $\mathcal{P}_{IQ1} = \mathcal{P}_{IQ2} = 0$ dB together with an additional phase shift $\phi_{IQ1} = \phi_{IQ2} = 0°$. We have found that the minimal transmission in the interrogating frequency range $\omega \in [6.5, 7]$ GHz is $T_{cal} = 0.0442$ which incorporates losses from the T-junction, microwave cables, insertion loss of the IQ-modulator, and the losses associated with the double-passing through the circulators. Another source of energy loss (which is already included in these measurements) is associated with the open and short terminators. We have used the terminators from a VNA calibration kit (Rhode & Schwarz ZV-Z235). The measurements have been repeated for different IQ-modulator values and the measured $S_{i1}^{(cal)}$ spectra showed the corresponding power reduction and phase shifts. The transmission used to evaluate the absorbance has then been normalized by $S_{i1} = S_{i1}^{(exp)} / \sqrt{T_{cal}}$. This choice of normalization underestimates the experimental absorbance, thus guaranteeing a conservative estimation of our measurements.

## Data availability

The data presented in this paper are available from the corresponding author upon reasonable request.

## Code availability

Codes used in this paper are available from the corresponding author upon reasonable request.

## References

1. Mei, J. et al. Dark acoustic metamaterials as super absorbers for low-frequency sound. *Nat. Commun.* **3**, 756 (2012).
2. Ma, G., Yang, M., Xiao, S., Yang, Z. & Sheng, P. Acoustic metasurface with hybrid resonances. *Nat. Mater.* **13**, 873 (2014).
3. Salisbury, W. W. Absorbent body for electromagnetic waves. US Patent 2599944 A (1952).
4. Landy, N. I., Sajuyigbe, S., Mock, J. J., Smith, D. R. & Padilla, W. J. Perfect metamaterial absorber. *Phys. Rev. Lett.* **100**, 207402 (2008).
5. Pham, V. T. et al. THz-metamaterial absorbers. *Adv. Nat. Sci. Nanosci. Nanotechnol.* **4**, 015001 (2013).

6. Cai, M., Painter, O. & Vahala, K. J. Observation of critical coupling in a fiber taper to a silica-microsphere whispering-gallery mode system. *Phys. Rev. Lett.* **85**, 74 (2000).

7. Piper, J. R. & Fan, S. Total absorption in a graphene monolayer in the optical regime bycritical coupling with a photonic crystal guided resonance. *ACS Photonics* **1**, 347 (2014).

8. Sturmberg, B. C. P. et al. Total absorption of visible light in ultrathin weakly absorbing semiconductor gratings. *Optica* **3**, 556 (2016).

9. Zhou, H. et al. Perfect single-sided radiation and absorption without mirrors. *Optica* **3**, 1079 (2016).

10. Baranov, D. G., Krasnok, A., Shegai, T., Alù, A. & Chong, Y. Coherent perfect absorbers: linear control of light with light. *Nat. Rev. Mater.* **2**, 17064 (2017).

11. Fante, R. L. & McCormack, M. T. Reflection properties of the Salisbury screen. *IEEE Trans. Ant. Prop.* **36**, 1443 (1988).

12. Vinoy, K. J. & Jha, R. M. *Radar Absorbing Materials* (Springer US, 1996).

13. Kats, M. A. & Capasso, F. Optical absorbers based on strong interference in ultra thin films. *Laser Photonics Rev.* **10**, 735 (2016).

14. Liu, N., Mesch, M., Weiss, T., Hentschel, M. & Giessen, H. Infrared perfect absorber and its application as plasmonic sensor. *Nano Lett.* **7**, 2342 (2010).

15. Kravets, V. G. et al. Singular phase nano-optics in plasmonic metamaterials for label-free single-molecule detection. *Nat. Mater.* **12**, 304 (2013).

16. Konstantatos, G. & Sargent, E. H. Nanostructured materials for photon detection. *Nat. Nano.* **5**, 391 (2010).

17. Knight, M. W., Sobhani, H., Nordlander, P. & Halas, N. J. Photodetection with active optical antennas. *Science* **332**, 702 (2011).

18. Zhang, J. F., MacDonald, K. F. & Zheludev, N. I. Controlling light-with-light without nonlinearity. *Light Sci. Appl.* **1**, 18 (2012).

19. Fang, X., MacDonald, K. F. & Zheludev, N. I. Controlling light with light using coherent metadevices: all-optical transistor, summator and invertor. *Light Sci. Appl.* **4**, e292 (2015).

20. Zhao, H. et al. Metawaveguide for asymmetric interferometric light-light switching. *Phys. Rev. Lett.* **117**, 193901 (2016).

21. Chong, Y. D., Ge, L., Cao, H. & Stone, A. D. Coherent perfect absorbers: time-reversed lasers. *Phys. Rev. Lett.* **105**, 053901 (2010).

22. Wan, W. et al. Time-reversed lasing and interferometric control of absorption. *Science* **331**, 889 (2011).

23. Fyodorov, Y. V., Suwunnarat, S. & Kottos, T. Distribution of zeros of the *s*-matrix of chaotic cavities with localized losses and coherent perfect absorption: non-perturbative results. *J. Phys. A* **50**, 30LT01 (2017).

24. Li, H., Suwunnarat, S., Fleischmann, R., Schanz, H. & Kottos, T. Random matrix theory approach to chaotic coherent perfect absorbers. *Phys. Rev. Lett.* **118**, 044101 (2017).

25. Chen, L., Kottos, T. & Anlage, S. M. Perfect absorption in complex scattering systems with or without hidden symmetries. *Nat. Commun.* **11**, 5826 (2020).

26. Pu, M. et al. Ultrathin broadband nearly perfect absorber with symmetrical coherent illumination. *Opt. Express* **20**, 2246 (2012).

27. Yoon, J. W., Koh, G. M., Song, S. H. & Magnusson, R. Measurement and modeling of a complete optical absorption and scattering by coherent surface plasmon-polariton excitation using a silver thin-film grating. *Phys. Rev. Lett.* **109**, 257402 (2012).

28. Bruck, R. & Muskens, O. L. Plasmonic nanoantennas as integrated coherent perfect absorbers on SOI waveguides for modulators and all-optical switches. *Opt. Express* **21**, 27652 (2013).

29. Roger, T. et al. Coherent perfect absorption in deeply subwavelength films in the single-photon regime. *Nat. Commun.* **6**, 7031 (2015).

30. Wong, Z. J. et al. Lasing and anti-lasing in a single cavity. *Nat. Photon.* **10**, 796 (2016).

31. Pichler, K. et al. Random anti-lasing through coherent perfect absorption in a disordered medium. *Nature* **567**, 351 (2019).

32. Sun, Y., Tan, W., Li, H.-q, Li, J. & Chen, H. Experimental demonstration of a coherent perfect absorber with PT phase transition. *Phys. Rev. Lett.* **112**, 143903 (2014).

33. Schindler, J. et al. $\mathcal{PT}$-symmetric electronics. *J. Phys. A* **45**, 444029 (2012).

34. Wei, P., Croënne, C., Chu, S. T. & Li, J. Symmetrical and anti-symmetrical coherent perfect absorption for acoustic waves. *Appl. Phys. Lett.* **104**, 121902 (2014).

35. Romero-García, V. et al. Perfect and broadband acoustic absorption by critically coupled sub-wavelength resonators. *Sci. Rep.* **6**, 19519 (2016).

36. Müllers, A. et al. Coherent perfect absorption of nonlinear matter waves. *Sci. Adv.* **4**, eaat6539 (2018).

37. Reddy, K. N., Gopal, A. V. & Gupta, S. D. Nonlinearity induced critical coupling. *Opt. Lett.* **38**, 2517 (2013).

38. Achilleos, V., Richoux, O. & Theocharis, G. Coherent perfect absorption induced by the nonlinearity of a Helmholtz resonator. *J. Acoust. Soc. Am.* **140**, EL94 (2016).

39. El-Ganainy, R. et al. Non-Hermitian physics and PT symmetry. *Nat. Phys.* **14**, 11 (2017).

40. Feng, L., El-Ganainy, R. & Ge, L. Non-Hermitian photonics based on parity-time symmetry. *Nat. Photon.* **11**, 752 (2017).

41. Miri, M.-A. & Alù, A. Exceptional points in optics and photonics. *Science* **363**, 7709 (2019).

42. Özdemir, Ş. K., Rotter, S., Nori, F. & Yang, L. Parity-time symmetry and exceptional points in photonics. *Nat. Mater.* **18**, 783 (2019).

43. Reisner, M. et al. Self-shielded topological receiver protectors. *Phys. Rev. Appl.* **13**, 034067 (2020).

44. Jeon, D. H., Reisner, M., Mortessagne, F., Kottos, T. & Kuhl, U. Non-hermitian CT-symmetric spectral protection of nonlinear defect modes. *Phys. Rev. Lett.* **125**, 113901 (2020).

45. Bellec, M., Kuhl, U., Montambaux, G. & Mortessagne, F. Tight-binding couplings in microwave artificial graphene. *Phys. Rev. B* **88**, 115437 (2013).

46. Sweeney, W. R., Hsu, C. W., Rotter, S. & Stone, A. D. Perfectly absorbing exceptional points and chiral absorbers. *Phys. Rev. Lett.* **122**, 093901 (2019).

## Author contributions

T.K. and U.K. designed and supervised the study. S.S. and Y. T. contributed equally to the development of the theory and numerical simulations. S.S. modeled the experimental data. T.K. supervised the theoretical work and modeling of experimental data. U.K., F.M., and M.R. designed the experimental setup, performed the experiments, and the experimental data analysis. T.K. and U.K. wrote the manuscript with input from all authors.

## Competing interests

The authors declare no competing interests.

## Additional information

**Supplementary information** The online version contains supplementary material available at https://doi.org/10.1038/s42005-021-00782-2.

**Correspondence** and requests for materials should be addressed to Ulrich Kuhl or Tsampikos Kottos.

**Peer review information** *Communications Physics* thanks Andrea Alu and the other, anonymous, reviewer(s) for their contribution to the peer review of this work.

**Reprints and permission information** is available at http://www.nature.com/reprints

**Publisher's note** Springer Nature remains neutral with regard to jurisdictional claims in published maps and institutional affiliations.